Research Square

Preprints are preliminary reports that have not undergone peer review.
They should not be considered conclusive, used to inform clinical practice,
or referenced by the media as validated information.

Electrophysiological and molecular characterization of a TGF-β1 goat model

Misha Regouski
Utah State University
Jens Fillmore
Utah State University
Raquel Larsen
Utah State University
Cheyenne Marriott
Utah State University
Tayler Patrick
Utah State University
Alexis Sweat
Utah State University
Rusty Stott
Utah State University
Aaron Thomas
Utah State University
Arnaud Wettere
Utah State University
Michael J. Cutler
Intermountain Medical Center
Heloisa M. Rutigliano
Utah State University
Irina A. Polejaeva
irina.polejaeva@usu.edu

Utah State University

Research Article

Keywords:

Posted Date: July 8th, 2026

DOI: https://doi.org/10.21203/rs.3.rs-10232704/v1

License: This work is licensed under a Creative Commons Attribution 4.0 International License.
Read Full License

Additional Declarations: No competing interests reported.

Version of Record: A version of this preprint was published at Transgenic Research on November 6th, 2026. See the published version at https://doi.org/10.1007/s11248-026-00517-5.

Abstract

Atrial Fibrillation (AF) is the most common cardiac arrhythmia in adult humans. Atrial fibrosis plays a primary role in developing and sustaining this disease phenotype. Specifically, TGF-β1, a potent pro-fibrotic molecule, is implicated in cell turnover, increasing the amount of extracellular matrix in the heart. This increase leads to aberrant electrical signaling and can produce AF.

In this study, we hypothesized that TGF-β1 modulates AF susceptibility in TGF-β1 transgenic goats and that genes related to TGF-β1 and AF would be differentially expressed when compared to wild-type (WT) controls. Transgenic (TG) female goats expressing the active form of human TGF-β1 in an atrial-specific manner and age-matched wild-type female goats were utilized in the study. Pacemakers were implanted in all animals for continuous arrhythmia monitoring and AF inducibility, which was evaluated using five separate 10s bursts of atrial pacing (200–160 ms). Tissue samples were collected from both atria of TG and WT goats. RNA was extracted, and gene expression analyses were run on a selected panel of genes. Immunohistochemistry was performed on atrial tissue to evaluate for the presence of selected inflammatory markers to elucidate AF substrate in these animals.

There was a significant increase in AF inducibility in both frequency and duration in TGF-β1 goats compared to their WT counterparts. There was no significant difference in the number of inflammatory cells tested by immunohistochemistry. Differentially expressed genes between the TG and WT groups were found in several functional categories including AF, apoptosis, extracellular matrix, inflammation, and TGF-β1.

These data support the hypothesis that fibrosis is an important modulator of AF susceptibility. More specifically, an overexpression of TGF-β1 significantly increases expression levels of ECM proteins and TGF-β1 signaling modulators, adding to elevated AF risk without altering underlying inflammation.

Introduction

The development of transgenic large animal models of atrial fibrillation (AF) provides a unique platform to study cardiac fibrosis and its implications on AF. To better understand the molecular underpinnings of AF, animal models can provide crucial data at the tissue and cellular levels without the complex ethical issues associated with human studies. Human cardiac tissue is often difficult to procure as typical availability includes only the atrial appendage, which is small and may not be indicative of whole chamber conductivity, or tissue that has been metabolically inactive for an extended period of time. Recent advancements in *in vivo* imaging have progressed in their usefulness but still have limitations in understanding molecular mechanisms of AF pathology (Olsen 2016). This leaves space for utilizing new technologies to produce large animal models that can provide adequate tissue and imaging capabilities which can then be translated to human medicine.

Our group developed a transgenic (TG) goat model of cardiac fibrosis. Fibrosis is a substrate in the pathogenesis of AF as a fibrotic substrate fosters aberrant electrical conductivity, which is thought to

contribute to the phenotype (Frangogiannis 2019). AF occurs when the atria develop rapid disorganized electrical activity and can this develop secondary to structural changes such as fibrotic patches in the heart leading to aberrant electrical stimulation and ectopic activity of atrial myocytes causing spontaneous depolarization (Brundel 2022). This spontaneous depolarization causes portions of the atria to randomly contract out of concert with itself and the ventricles. Significant research has focused on aberrant electrical activity caused by structural remodeling, such as fibrosis. As such, when developing this TG goat model, progressive fibrosis was paramount to mimic the human progression of the disease (Polejaeva 2016). Although TG goats exhibit higher AF susceptibility compared to wild-type (WT) controls, further information at the molecular level is needed to understand the role fibrosis plays in AF.

Previously, this model has been shown to exhibit spontaneous AF when exposed to environmental stressors, such as endurance exercise (Regouski 2019). Additionally, ex-vivo cardiac magnetic resonance imaging studies have shown slower atrial conduction speeds and disorganized fibrotic patches when compared to WT control goat hearts (Kwan 2024). Thus, several studies evaluating the role of fibrosis in this goat model have shown an increased AF susceptibility, and even episodes of spontaneous AF, but expression of key genes associated with fibrosis has not been evaluated. Therefore, understanding key molecular pathways involving inflammation and TGF-β is crucial to gain further understanding into this model's capabilities of recapitulating AF with underlying fibrosis as the substrate.

The crux of using TGF-β1 as a modulator of cardiac fibrosis lies in its ability to promote fibrosis while also being anti-inflammatory. Routine insult to tissue typically results in higher local and circulating inflammatory markers (Wynn 2012). However, TGF-β1 overexpression results in higher fibrosis by inducing differentiation of fibroblasts into myofibroblasts and secreting excessive amounts of ECM (Bolivar 2021) while maintaining an overall global anti-inflammatory effect. Investigating the link between non-inflammatory fibrosis in the atria and AF occurrence can determine if fibrosis alone is enough to sustain AF. To generate this model, we produced genetically modified goats via somatic cell nuclear transfer (SCNT) using cells containing a cardiac specific overexpression of TGF-β1. This modification leads to diffuse fibrosis in the atria (Polejaeva 2016).

The present study aimed to compare the expression of genes related to the TGF-β1 pathway, inflammation, fibrosis, apoptosis, and atrial fibrillation, the presence of inflammatory cells and the occurrence of AF between TG goats and their WT counterparts to help elucidate the role cardiac fibrosis has on the molecular and electrophysiologic properties of the TG goat heart. We hypothesized TG goats would have an upregulation of transcript levels in most gene categories, with the exception of genes related to inflammation as TGF-β1 has anti-inflammatory properties (de Oliveira 2021). This molecular and cellular profiling may help in understanding the role that fibrosis plays in the pathogenesis of AF in this model and may glean insight into clinical cases of AF with a fibrotic cause.

Materials and Methods

Animals

Procedures were approved and conducted by the published guidelines by Utah State University Institutional Animal Care and Use Committee (IACUC). Twelve female adult domestic goats (*Capra hircus)* between two and seven years of age were used in this study. The six TG animals used have overexpression of human TGF-β1 in atrial tissue and come from a Nubian Boer cross background. The six WT goats used were Spanish Nubian crosses. The generation of human TGF-β1 transgenic goats is described in detail by Polejaeva et al. (Polejaeva 2016). Briefly, a cardiac specific α-myosin heavy chain (αMHC) promoter was subcloned into the pcDNA3.1D vector. The Invitrogen NEON transfection (Invitrogen, Waltham, MA, USA) was used to electroporate primary goat fetal fibroblasts. Cells containing the transgene were used for SCNT and were screened by polymerase chain reaction (PCR) to confirm the presence of the transgene. Oocytes were collected as described elsewhere (Yang 2016). SCNT, recipient synchronization, and embryo transfers were performed as described by our laboratory team (Yang 2018). Once recipients gave birth, clones were screened via PCR^5 to ensure the construct was wholly intact and allowed to mature to at least 18 months of age before being utilized on any study. Our group has characterized this model previously, showing an increased P wave duration, increased ECM in the atria, and inducible AF episodes (Polejaeva 2016, Regouski 2019).

Pacemaker Implantation

Dual chamber pacemakers were implanted into the right atrium of TG and WT goats that were between two and seven years old. Anesthesia was induced in goats undergoing implantation with a combination of Ketamine (6 mg/kg) and Diazepam (0.1–0.2 mg/kg) administered intravenously (IV) via the jugular vein. Immediately following induction, animals were intubated, and anesthesia was maintained with isoflurane dosed to effect (2–4%) in inspired oxygen. The surgical site was scrubbed with three alternating washes of a chlorhexidine scrub followed by isopropyl alcohol. As part of the preparation, each animal received Cefazolin, 20 mg/kg, IV intraoperatively to reduce the risk of bacterial infection arising during the procedure, as well as a lavage of cefazolin at the generator implant site. Pacemakers were generously donated by Boston Scientific, and either their Accolade or Altrua model platform (Boston Scientific, 300 Boston Scientific Way, Marlborough, MA) was used. Pacemaker leads were introduced into the right atria through a cutdown to the right jugular vein. The leads were tunneled subcutaneously and attached to a pacemaker generator in a separate site on the neck. Leads were visualized using C-arm fluoroscopy for correct orientation and insertion into the right atrial wall. Conductivity was tested immediately post-implantation and any lead revisions were performed as necessary. The incision was closed, and the animals were carefully monitored during recovery. Animals were provided with post-operative analgesia by a single injection of flunixin meglumine (1.1 mg/kg administered IV). Standard postoperative care such as bandage checks and antibiotic administration was performed daily until the incisions healed. Lead stability was tested one-week post-procedure, and revisions were performed as necessary. Although no goats experienced post-operative infections and incisions were healed within a week, no study was started until two months post-surgery.

AF Induction

Burst pacing for 10 seconds at varying milliseconds (160–200) was performed: once at 200mS, two at 180mS, and two at 160mS. AF inducibility was assessed by recording the number of AF episodes and their durations at each burst. Goats were allowed to self-terminate any AF episodes recorded. No spontaneous episodes were noted during the baseline experimental phases. TG goats assessed for AF inducibility were all between four and seven years of age and had age-matched WT animals as a comparison. All animals weighed between 45 and 73 kilograms. Baseline inducibility was performed twice two weeks apart on each goat.

Sample Collection

Goats were euthanized according to current American Veterinary Medical Association guidelines with an intravenous injection of phenobarbital at a 20mg/kg dose. Hearts were excised from the chest immediately upon confirming the lack of heartbeat and corneal response. Cardiac muscle tissue from left and right atria (LA and RA) were snap-frozen in liquid nitrogen for RNA isolation. Additionally, the same tissue types were placed into optimal cutting temperature compound (OCT) in plastic boats submerged in chilled isopentane and stored at -80° C as well as formaldehyde for histological analysis. Reagents detailed below were all obtained from Thermo Fisher Scientific (*Thermo Fisher, Waltham, MA)* unless otherwise noted.

Immunohistochemistry

Atrial samples collected in OCT for immunohistochemistry (IHC) staining were processed using an in-house protocol (Koroghli 2018). Briefly, sections were removed from storage and allowed to air dry, sections of right atrium from each animal were cut at 20 µm on a cryostat, placed on glass slides and then stained for different immune cell populations. Antibodies were obtained from Washington State University's Monoclonal Antibody Center (WSU, Pullman WA) unless otherwise noted. Antibodies included MUC2A used at a 1:200 dilution for the CD2 antigen, 17D used at a 1:200 dilution for CD4 antigen, GB25A used at a 1:400 dilution for CD21, and finally, TH14B used at a 1:200 dilution for MHC-II antigen. Ten slides per cardiac chamber per animal were saturated with a 0.3% hydrogen peroxide solution, washed in phosphate-buffered saline (PBS), and then blocked in a 2% normal goat serum and 1% bovine serum albumin solution. Then, each slide set was incubated with a primary antibody at the working concentrations described above and rinsed in PBS. Incubation with a secondary antibody (biotinylated goat anti-mouse IgG [Vector Labs, Newark, CA, USA]) diluted in casein to 1:200 was introduced to the slides, after incubation, slides were rinsed in PBS. Streptavidin conjugate was placed on the slides, rinsed in PBS, and AEC chromogen was applied. Slides were rinsed in distilled water and then counterstained with Gill's #2 hematoxylin. Fluoromount G was applied, coverslips were placed and sealed with clear nail polish. Slides were then imaged using a Zeiss Axio Observer Z1 (Zeiss, Hebron, KY,

USA), ten fields of view at 40x objective were visualized for the presence of positive cells from antibody staining and the number of positive cells per area was recorded.

Histology

Formalin-fixed heart sections were collected, processed, and embedded in paraffin following routine histological techniques. 5µm thick sections were stained with Masson's Trichrome stain according to standard methods and evaluated under light microscopy. Images were obtained using an Olympus BX 43 microscope with a 40X objective. Fibrosis amounts were determined by measuring the area occupied by blue staining (collagen) using Phtoshop. A manual threshold was set and those settings were used on all images to determine the area percent of fibrosis.

Gene Expression

The Fluidigm Biomark system (Standard Biotools, San Francisco, CA, USA) was used for gene expression analysis. Snap frozen tissue was used from each atrium for RNA extraction. Purified RNA samples were converted to cDNA for use in this manner as follows. The RNeasy mini kit (Qiagen, Germantown, Maryland, USA) was used according to the manufacturer's protocol. A QIAzol/chloroform purification step was added as the nature of cardiac tissue proved difficult for high-quality RNA isolation without this additional step. Tissue pieces weighing 20 mg +/-2mg from both atria from all animals were placed into QIAzol (Qiagen, Germantown, Maryland, USA) and homogenized. Chloroform was added, and the samples were spun to separate out total RNA. The samples were then placed into spin columns provided in the kit, ethanol was added, and several wash steps followed. Finally, RNA was eluted in RNase-free water. Sample concentration was determined using a Nanodrop 2000 spectrophotometer.

RNA samples were diluted to 0.5µg/µL in DNA suspension buffer and converted to cDNA using a VILO cDNA synthesis kit wherein diluted mRNA was mixed with the proprietary superscript master mix enzyme and incubated on a thermocycler for 10 minutes at 25° C, 10 minutes at 50° C, and five minutes at 85° C. Primers were designed using NCBI blast data and efficiency was determined using stepwise dilutions from 1:100 up to 1:10000. Primers and samples were run in duplicate, producing four replicates of each sample/primer combination. Primer sequences and efficiencies can be found in Table 1, efficiencies lower than 85% were excluded.

Table 1
Genes selected for real-time qPCR analysis, their functional categories, primer sequences and efficiencies.

Gene	Gene Name	Primer Sequence	Efficiency
TGFβ Signaling Genes			
ALK1	Activin receptor like kinase 1	TGCTGCTCAGACACGACAA CTCGAGTTGCGGGAAGTCA	95%
ALK3	Activin receptor like kinase 3	TGGCAGTGGATCTGGACTAC CTTTACCAACTTGCCGAACCA	94%
BMP4	Bone morphogenic protein 4	GGCATCGGTCTGGAGTATCC GGTCCCTGGGATGTTCTCC	94%
BMP6	Bone morphogenic protein 6	CGACATCCCTTCTCCTCAAGAA AGGGGAGAACTCCTTGTCGTA	95%
hTGFβ	Human transforming growth factor beta	GCGTGCTAATGGTGGAAACCCA GCTGTGTGTACTCTGCTTGAAC	86%
LOX	Lysyl Oxidase	TGGTGCCCGATCCCTACTAC GCAGCGCATCTCAGGTTGTA	91%
LTBP2	Latent transforming growth factor beta binding protein 2	GACGGGTGACTGCATTGACA CCGTCGGTGTTGTCACAGAA	95%
LTBP3	Latent transforming growth factor beta binding protein 3	GATGGCACTGCTGCCTTCA GTGGGAGGTGAGGATGTGGTA	95%
MKP1	Map kinase phosphatase 1	TTGCTGATGTGCCAGACCAA GCCGTTGACACACCATTTCC	93%
SMAD2	Mothers against decapentaplegic homolog 2	ACCACTACCAGAGAGTTGAGAC GGGCAGTTCTGTTAGGATCTCA	94%
SMAD3	Mothers against decapentaplegic homolog 3	AGCCCCAGAGCAATATTCCA GTGGTTCATCTGGTGGTCAC	94%
Extra Cellular Matrix Genes			
COL1A1	Collagen type I alpha 1 chain	TGGTGCTGACGGACCTGCT CACACCACGCTGTCCAGCAA	80%

Gene	Gene Name	Primer Sequence	Efficiency
TGFβ Signaling Genes			
COL1A2	Collagen type I alpha 2 chain	CTGGTGAGCCTGGTGAACCT CATCCTCACCAGCCTTGCCA	96%
COL3A1	Collagen type III alpha 1 chain	CACGCAAGGCCGTCAGACTA AGGGCCAATGTCCGCACCA	95%
FN1	Fibronectin 1	CACACCCTTGACTCCTGTTGT CTCTTCACTCAGCTCATACTCCA	89%
MMP2	Matrix metalloprotein 2	CCATGATGGAGAGGCTGACA GCCCGTCTTTGCCATCAAA	89%
Apoptosis			
BAX	BCL 2 like protein	TGGCGGCTGAAATGTTTTCC CCAGTTTGCTGGCAAAGTAGAA	89%
Inflammation Genes			
CD105	Endoglin	CCACCCCAATGAACCTTCAAAC TACAGGGCAGTGGACTCTCA	95%
IFNg	Interferon gamma	GATAACCAGGTCATTCAAAGGAGC GATCATCCACCGGAATTTGAATC	93%
IGF2	Insulin like growth factor 2	CCGCTGTTCGGTTTGCAATA TGATCCCCATTGATGTCTGGAA	94%
IL1	Interleukin 1	GCCTTCAATAACTGTGGAACCAAT GTATATTTCAGGCTTGGTGAAAGGA	91%
IL4	Interleukin 4	GGCGTATCTACAGGAGCCACAC CAAGAGGTCTTTCAGCGTACTTGT	92%
IL5	Interleukin 5	TGGTGGCAGAGACCTTGACA GAATCATCAAGTTCCCATCACCTA	93%
IL6	Interleukin 6	GGCTCCCATGATTGTGGTAGTT GCCCAGTGGACAGGTTTCTG	93%
IL8	Interleukin 8	GGAAAAGTGGGTGCAGAAGGT	86%

Gene	Gene Name	Primer Sequence	Efficiency
TGFβ Signaling Genes			
		GGTGGTTTTTTCTTTTTCATGGA	
IL10	Interleukin 10	GAGCAAGGCGGTGGAGAAGG	89%
		GATGAAGATGTCAAACTCACTCATGG	
IL15	Interleukin 15	GGGCTGTATCAGTGCAAGTCTTC	85%
		ATTGGGATGAGCATCACTTTCAG	
TNFα	Tumor Necrosis Factor alpha	TCTACCAGGGAGGAGTCTTCCA	92%
		GTCCGGCAGGTTGATCTCA	
Atrial Fibrillation Genes			
CX43	Connexin 43	GGGCTTGCTGAGAACCTACA	94%
		TGTACCACTGGATCAGCAAGAA	
KCNA1	Potassium voltage-gated channel subfamily A member 1	AGCTGAAGGACGAGAAGGAC	94%
		CGTGAAGATGTTGGCGTTGTA	
KCNIP1	Potassium voltage-gated channel interacting protein 1	CCTTCTCCTCTCTGCAAACC	85%
		GCAAACCATGGTCATCTCCA	
SHOX2	Short stature homeobox 2	GGACCAATTTCACCCTGGAA	94%
		GGCTCAGTTCTTCACGCATA	
SNAIL1	Zinc finger protein SNAI 1	TGCCCTCAAGATGCACATCC	91%
		CCTTCCCGCAGGTGCTAC	
TIMP1	Metallopeptidase inhibitor 1	ACCGCAGAAGTCAATGAGAC	95%
		AGGCACTGAACCCTTTGAAC	

Statistical Analyses

Statistical differences were assessed with a Student's t-test for baseline inducibility between WT and TG animals after data was checked for normal distribution. Gene expression data were assessed using a repeated measures ANOVA test (Park 2009) for atrial chamber effect and treatment (TG vs WT) effect. A false discovery rate (FDR) test was applied to the gene expression data to correct for multiple comparisons (Benjamini 2018). Adjusted *p* values can be found in Table 2. Immunohistochemistry data was assessed using a Student's t-test. A Mann-Whitney U test was used for histological analysis. All

data are expressed as mean ± standard error of the mean (SEM). Statistical data analysis was performed using Jamovi (The Jamovi Project (2022). *jamovi* (Version 2.3).

Table 2
False Discovery Rate Analysis for genes analyzed via real-time qPCR

Gene	RM ANOVA *p* value	FDR adjusted *p* value	Rank
KCNIP1	0.0000000000010871	0.0000000000380485	1
IL8	0.0000000000062028	0.0000000001085490	2
IL5	0.0000000000068497	0.0000000000799132	3
IL10	0.0000000000071367	0.0000000000624461	4
SHOX2	0.0000000000091402	0.0000000000639814	5
IFNG	0.0000000000243010	0.0000000001417558	6
SNAIL1	0.0000000000264583	0.0000000001322915	7
IL15	0.0000000001478110	0.0000000006466731	8
KCNA1	0.0000000004016549	0.0000000015619913	9
IL6	0.0000000010741329	0.0000000037594652	10
LTBP2	0.0000000049462419	0.0000000157380424	11
IL1	0.0000000083553700	0.0000000243698292	12
BMP6	0.0000000777210000	0.0000002092488462	13
TNFa	0.0000001067615926	0.0000002669039815	14
BMP4	0.0000001126556000	0.0000002628630667	15
SMAD3	0.0000001593773135	0.0000003486378733	16
TGFB	0.0000002203534906	0.0000004536689512	17
ALK3	0.0000003158398000	0.0000006141329444	18
TIMP1	0.0000011403295448	0.0000021006070562	19
SMAD	0.0000014469365703	0.0000025321389980	20
HTGFB	0.0000026470000000	0.0000044116666667	21
MKP1	0.0000036115831614	0.0000057457004840	22
ALK1	0.0000038702000000	0.0000058894347826	23
LTBP3	0.0000038822575777	0.0000056616256341	24
CD105	0.0000062939700000	0.0000088115580000	25
FN1	0.0000071010000000	0.0000095590384615	26
IGF2	0.0000085583390000	0.0000110941431481	27

Gene	RM ANOVA *p* value	FDR adjusted *p* value	Rank
MMP2	0.0000088011883954	0.0000110014854943	28
CX43	0.0000166436000000	0.0000200871034483	29
LOX	0.0000200280145894	0.0000233660170210	30
GTGFB	0.0000545720000000	0.0000616135483871	31
COL1A2	0.0001259043000000	0.0001377078281250	32
COL3A1	0.0002685372970000	0.0002848122846970	33
COL1A1	0.0025351655000000	0.0026097291911765	34
IL4	0.7544071588200000	0.7544071588200000	35

A false discovery rate test was applied to genes used for qRT-PCR analysis. Initial *p* values are reported in addition to adjusted *p* values.

Results

Inducibility

A significant difference using a Student's t-test between the inducibility of TG and WT animals was found with a *p*-value of 0.04 (Fig. 1). TG goats, on average, had episodes lasting 51.30 ± 29.27 seconds, whereas WT goats only had episodes lasting 8.98 ± 3.18. This shows that the TG animals have a higher level of AF susceptibility than their age and sex-matched WT controls.

Figure 1. Average atrial fibrillation (AF) duration of TGF-β1 transgenic animals (TG, n = 6) when compared to their wild-type (WT, n = 6) controls. Average duration in seconds at baseline is significantly upregulated in TG animals when compared to their WT controls, as denoted by the symbol *. WT animals had an average induced AF duration of 8.98 ± 3.18 seconds, whereas TG animals had an average of 51.30 ± 29.27 seconds (*p* = 0.04) when analyzed using a Student's t-test. Data are expressed as mean ± SEM.

Immunohistochemistry and Masson's Trichrome Staining

As shown in Figs. 2 and 3, there were no significant differences between TG and WT goats in the number of inflammatory cells (CD2 [T cells], CD4 [helper T cells], CD21 [B cells], and MHC-II [antigen-presenting cells] in the atria. Figure 4 shows representative images of Masson's Trichrome staining of TG and WT atria where a significant difference in percent fibrosis between groups was observed.

Figure 2. Analysis of immune cell populations in the right atrium of human TGF-β1 transgenic (TG, n = 6) goats compared to age and sex matched wild-type (WT, n = 6) control goats via immunohistochemistry staining. No significant differences were found between groups using a Student's t-test. The number of T

cells (CD2+) had a significance level of *p = 0.19*, the number of T helper cells (CD4+) had a significance level of *p = 0.13*, the number of B cells (CD21+) had a significance level of *p = 0.36*, and finally, the number of antigen-presenting cells (MHC-II+) had a significance level of *p = 0.39*. Data are presented as average ± SEM.

Figure 3. Immunohistochemical labeling of cells for CD2, CD4, CD21, and MHC-II in the atrium of TGF-β1transgenic (TG) and age and sex matched wild-type (WT) control goat atrial samples. Using a Zeiss Axio Observer Z1 (Zeiss, Hebron, KY, USA) microscope, ten fields of view at 400x objective were visualized for the presence of positive cells from antibody staining and the number of positive cells per area was recorded.

Figure 4. Representative images of Masson's Trichrome staining of atrial tissue from two TGF-β1transgenic goats in panel A and B and two age and sex matched wild-type control goat atrial tissue in panel C and D. 40x scale bar=500μm. Images were analyzed using Photoshop to obtain the percent fibrosis. Using the Mann-Whitney U test, percent fibrosis was significantly higher in TG hearts (TG, n = 8) compared to WT controls (WT, n = 7): median [IQR]: TG 6.5% (4–9%), WT 2% (0–2%), U = 56, *p* = 0.0014.

Gene Expression

Several genes were significantly differentially expressed in the TG group when compared to the WT group of goats using repeated measures ANOVA. Many differences were found in varying functional categories, including genes implicated in AF, TGF-β1 pathway, ECM, and inflammation. No differences were found in the apoptotic gene category. Glyceraldehyde-3-phosphate dehydrogenase (GAPDH) and actin beta (ACTB) were used as housekeeping genes to normalize genes of interest to. These two genes were selected for their stable expression and efficiency determined by cycle thresholds between 23 and 28 and efficiencies of 94% and 92% respectively.

Significant differences between TG and WT goat groups are shown in Figs. 5–8. Specifically, *KCNA1, KCNIP1*,and *SHOX2*, in the AF gene category, were all significantly downregulated, while CX43 was upregulated when compared with WT animals. *ALK1, ALK3, hTGF-β, LOX, LTBP3, MKP-1*, and *SMAD* were significantly upregulated in TG animals compared to WT. In the inflammation category, only *CD105* and *IGF2* were significantly upregulated, while *IFNγ, IL1, IL5, IL8, IL10, IL15*, and *TNFα* were significantly downregulated in TG animals when compared to WT. Lastly, the ECM category yielded several upregulated genes, including *COL1A1, COL1A2, COL3A1, FN1*, and *MMP2*.

Figure 5. Fold change of gene expression of atrial fibrillation (AF) related genes showing significant difference between TGF-β1transgenic (TG; n = 6) and age and sex matched wild-type (WT; n = 6) control goat atrial samples. Graphs represent 2^-ΔΔCT fold change in relative mRNA transcript levels in TG animals detected using qRT-PCR, values were normalized to mRNA transcript levels of glyceraldehyde-3-phosphate dehydrogenase (GAPDH) and actin beta (ACTB) and to WT animal transcript level for the individual target gene. After a false discovery rate adjustment of significant values, and a fold change cut

off of 1.5 applied: CX43 has a significance level of *p = 0.003 KCNA1 p = 0.012, KCNIP1 p = 0.009, SHOX2 p = 0.02.* Non-adjusted *p* values can be found in Table 2. Data are expressed as mean ± SEM.

Figure 6. Fold change of gene expression of TGFβ-1 related genes showing significant difference between TGF-β1transgenic (TG; n = 6) and age and sex matched wild-type (WT; n = 6) control goat atrial samples. Graphs represent 2^-ΔΔCT fold change in relative mRNA transcript levels in TG animals detected using qRT-PCR, values were normalized to mRNA transcript levels of glyceraldehyde-3-phosphate dehydrogenase (GAPDH) and actin beta (ACTB) and to WT animals transcript level for the individual target gene. After a false discovery rate adjustment of significant values and a fold change cut off of 1.5 applied, *ALK1* has a significance of *p = 0.003, ALK3 p = 0.002, hTGFβ p = 0.004, LOX p = 0.002, LTBP3 p = 0.002, MKP-1 p = 0.001, and SMAD* also had a significance level *of p = 0.001.* Non-adjusted *p* values can be found in Table 2. Data are expressed as mean ± SEM.

Figure 7. Fold change of gene expression of inflammation-related genes showing significant difference between TGF-β1 transgenic (TG; n = 6) and age and sex matched wild-type (WT; n = 6) control goat atrial samples. Graphs represent 2^-ΔΔCT fold change in relative mRNA transcript levels in TG animals detected using qRT-PCR, values were normalized to mRNA transcript levels of glyceraldehyde-3-phosphate dehydrogenase (GAPDH) and actin beta (ACTB) and to WT animal transcript level for the individual target gene. After a false discovery rate adjustment of significant values and a fold change cut off of 1.5 applied, *CD105* had of *p = 0.002, IFNγ p = 0.005, IGF2 p = 0.002, IL1 p = 0.001, IL5 p = 0.002,, IL8 p = 0.001, IL10 p = 0.004, IL15 P = 0.003 and TNFα* also had a significance level *of p = 0.001.* Non-adjusted *p* values can be found in Table 2. Data are expressed as mean ± SEM.

Figure 8. Fold change of gene expression of extra cellular matrix related genes showing significant difference between TGF-β1transgenic (TG; n = 6) and age and sex matched wild-type (WT; n = 6) control goat atrial samples. Graphs represent 2^-ΔΔCT fold change in relative mRNA transcript levels in TG animals detected using qRT-PCR, values were normalized to mRNA transcript levels of glyceraldehyde-3-phosphate dehydrogenase (GAPDH) and actin beta (ACTB) and to WT animal transcript level for the individual target gene. After a false discovery rate adjustment of significant values and a fold change cut off of 1.5 applied, *COL1A1* has a significance of *p = 0.003, COL1A2 p = 0.002, COL3A1 p = 0.002, FN1 p = 0.005, and MMP2* also had a significance level *of p = 0.001.* Non-adjusted *p* values can be found in Table 2. Data are expressed as mean ± SEM.

Discussion

This work builds upon the characterization of a TGF-β1 transgenic goat model of AF. The data show important distinctions between fibrosis and inflammation and their roles in the development and progression of AF. While we have previously established the inducibility and viability of this model (Polejaeva, 2016), this work investigates the mechanisms of AF that are not as feasible to investigate with laboratory animal models or human patients. Tissue from goats is similar to humans both in total volume and structure making this model a strong candidate for studying the role fibrosis plays in AF (Kay

1983). This helps elucidate a clearer picture of the pathophysiology of AF, in that, fibrosis without acute myocardial injury is a strong enough trigger to develop and sustain an AF phenotype. As mentioned previously, several genes were differentially expressed between TG and WT animals and seem to have a strong tendency to be associated with an AF phenotype, as discussed in further detail below.

The SMAD family of proteins is part of the TGF-β1 cascade and is implicated in the conversion of an inactive cell type, such as a fibroblast, into an activated myofibroblast cell type (Humeres 2022). *SMAD* and *SMAD3* were upregulated in the TG animals, this is expected as canonical TGF-β1 pathway activation occurs through intracellular SMAD activation (Frangogiannis 2020). Further research is needed to characterize the intricacies the SMAD family may have on TGF-β1 signaling. *ALK1* and *ALK3* are both involved in angiogenesis and cell-cell communication, the upregulation observed in TG goats could be due to new blood vessel formation due to extracellular matrix formation in the atria (Farhan 2022). This gene family is also implicated in TGF-β1 signaling as they are present in cellular membranes and act as binding sites for both TGF-β1 and SMAD proteins for activation of the pathway, as such, increased expression in TG animals is expected (Chen 2016). Evaluating this model of cardiac fibrosis via non-canonical TGF-β1 pathways (i.e. ERK, AKT, and MAPK) may be useful to understand if these pathways may contribute to fibrotic signaling in the atria of TG goats.

The bone morphogenic protein (BMP) gene superfamily is closely connected with TGF-β1 and its signaling pathway as they are mostly implicated in cardiac cell differentiation (de Pater 2012). In addition to cellular differentiation, the BMP family is also implicated in embryogenesis, apoptosis, organogenesis, and morphogenesis (Hogan 1996). BMP proteins are part of the SMAD-dependent signaling cascade of TGF-β1 and help bind to ligands that recruit various receptors leading to activation of the LLC of the latent TGF-β1 molecule (Boeuf 2012). We see differential expression with different types of BMP proteins within this family in our study. Specifically, *BMP4* and *BMP6* are involved in dimerization of the activated TGF-β1 molecule (Ye 2023).

As expected, the expression levels of TGF-β1 were increased in TG goats. This aligns with expectations, as TG goats were designed to over-express the molecule. The two variants of latent TGF-β1 binding protein selected as gene targets had a varied response in the TG animals. *LTBP3* is more directly involved in the TGF-β1 pathway and can only bind to the active form of TGF-β1 (Robertson 2015), the increased expression levels we see follow TGF-β1 expression in TG animals.

Collagens are the main constituent of the ECM and are vital to provide scaffolding structure to tissue. However, aberrant, increased levels of collagen can disrupt tissue functions. All three genes related to collagen deposition such as *COL1A1, COL1A2*, and *COL3A1* tested in this study had increased expression in the atrium of TG goats compared to WT goats. These genes promote fibrosis through ECM laydown and are linked with AF development (Polejaeva 2016, van den Berg 2021).

LOX is another common regulator of ECM. Its upregulation observed here shows its involvement in the increased ECM deposition in TG goats as it is found in higher levels in tissues with greater levels of fibrosis (Al-U'datt 2019). Quantifying insoluble ECM fractions in atrial tissue would be a valuable future

study to further define fibrotic remodeling in this model of cardiac fibrosis, given Lysyl Oxidase's role (*LOX)'* in structural remodeling of the atria. *MKP-1* is a complex gene implicated in various cardiac functions, namely cardiogenesis and the ERK1/2 growth factor pathway, which is implicated in cell turnover and fibroblast growth factor activation (Rose 2010). Increased expression levels in TG goats are most likely due to the conversion of inactive fibroblasts into activated myofibroblasts. Fibronectin 1 (*FN1*) also has a strong tie with regulating ECM laydown and has been previously identified to be elevated in human patients with AF (Büttner 2018). Our TG goats exhibiting higher levels of *FN1* than their WT counterparts is expected.

Voltage-gated potassium channels are not traditionally considered drivers of AF; however, an upregulation of potassium channel gene expression has been observed in patients with persistent AF (Glasscock 2015). *KCNIP1* expression is a strong indicator of the development of AF in humans via *KCNIP1'*s association with the L-type calcium current in the heart (Tsai 2016). *KCNIP1* significantly differed between TG and WT animals, with TG goats having a decreased expression level. This is puzzling, as we would have expected increased levels of *KCNIP1.* Further studies, such as CM patch clamping, or fluorescence-activated cell sorting (FACS) to isolate specific cell populations, should be performed to understand any ramifications TGF-β1 may have on ion channels and to understand how changes in cell population may contribute to the observed transcriptional differences. *KCNA1* was found to be significantly different between treatment groups. The downregulation of these genes could show a potential ionic mechanism for AF as a decrease in potassium transport, which impacts the repolarization of the CM, fosters shorter action potential durations causing a lack of arrhythmogenesis (Tsai 2016).

SHOX2 is a known genetic variant implicated in the development of AF (Hoffmann 2019). Much research is being done in gene and cell therapy to correct AF (Sumer 2020) with *SHOX2* variants. *SHOX2* is vital to the development of the sinoatrial (SA) node and has a large role in the embryogenesis of the cardiac conduction system. Mice with a *SHOX2 -/-* phenotype die at a young age from bradycardia due to a lack of specialized pacemaker cells (Hu 2018). Our gene expression data showed a significant decrease between TG and WT goats, most likely due to a variant of *SHOX2* being expressed. Further research is needed to explain this result. Connexin 43 was significantly upregulated in TG animals when compared to WT goats. Connexins are largely implicated in the electrical signaling of CMs. As non-specific membrane pores, connexins allow small molecules to be transported between cells and have strong ionic conductance allowing for electrical signal transmission between cells (Lambiase 2015). The heart can function because of the electrical signal propagation of these specialized units. Aberrant electrical signals are commonly found in AF, some of which are thought to result from improper connexin signaling either from a decrease in global connexin isoforms or differences in their distribution within the heart (Guo 2022). MMP2 was also upregulated in our TG goat when compared to the WT group and is implicated as a risk factor for recurring AF in humans, particularly when active TGF-β1 is also found to be upregulated and may be implicated in leukocyte transendothelial migration (Guan 2022, Li 2022).

KCNA1, KCNIP1, and *SHOX2* were significantly downregulated in the TG goats. This is likely due to different variants that would not be picked up by the designed primers. Further research into these

expression levels is needed to understand the downregulation in this animal model.

A common cytokine found to be pro-apoptotic is *IFNγ*, this cytokine is commonly found in cancers due to its response to immunological perturbations (Castro 2018). *IFNγ* is largely responsible for leukocyte attraction and cellular differentiation. Mice born without *IFNγ* show immunodeficiencies against bacterial, parasitic, and viral infections (Schroder 2004). Its role in AF is not fully understood, but there is supporting literature for its role in a profibrotic pathway and implicated in cell turnover (Zhou 2021). This supports the finding that TG goats exhibit a significant downregulation of *IFNγ* in cardiac tissue when compared to their WT counterparts, as there were no other significant differences found in apoptotic genes.

Overall, an increase in the gene expression of inflammatory markers, such as interleukins, was not an anticipated result. However, specific interleukin expression may offer some clues into the development of AF in TG goats. AF is thought to have a global inflammatory effect in cardiac muscle, supporting the idea that injury must be present for fibrosis to occur (Oikonomou 2019). Although IL-6 is commonly known as a pro-inflammatory cytokine, it is an anti-inflammatory myokine. That is when expressed from myocytes, it produces a localized anti-inflammatory effect through stimulating other anti-inflammatory cytokines (Petersen 1985). There is supporting data in human patients showing upregulation in the expression of *IL-6* in patients with lone, paroxysmal, and organic AF (Cheng 2012). Though there is contradictory literature, this highlights the complexity between inflammation and AF and any other factors the overexpression of TGF-β1 could have within the genetically engineered animals.

A previous mouse study shows a lower levels of *IL-1* and *IL-8* in the sera of mice with AF through thromboembolisms (Shan 2019), the data in our goats agrees. *CD105* is a common biomarker predictive of AF when found in atrial tissue, due to its role in angiogenesis post ischemic event in the heart. It is implicated in fibrosis and was found to be upregulated in TG goats compared to their WT counterparts (Gramley 2010). Insulin-like Growth Factor 2 (*IGF2*) is found in a myriad of fibrotic diseases (e.g. idiopathic pulmonary fibrosis, scar formation, liver, and renal fibrosis). The upregulation we found in TG goats is expected as one of its roles in a fibrotic disease state is excessive ECM deposition (Zhu 2022). Our results align with expectations with these upregulated genes and show that inflammation itself is not the primary driving factor for the development of AF in TG animals.

The lack of significance in apoptotic and decreased expression of inflammatory genes was unsurprising as no goats had any cardiac insult other than pacemaker implantation. Although cell death and inflammation are implicated in AF and can facilitate fibrosis (Hu 2015), our results are as expected as the fibrosis seen in TG animals is likely due to excess and active TGF-β1 expression. Acute inflammation, such as post operative AF (Heijman 2020) would be an unlikely candidate for fibrosis found in these animals as no experimental parameters would have introduced a sudden change to the substrate of the heart, such as an ablative intervention or other procedure. Though pacemaker implantation may have induced a localized increase of inflammatory markers no data were collected from the animals then. Chronic inflammation can occur when a continuous insult happens to cardiac tissue. Although certainly

a common driver for AF development, typically chronic inflammation is found as a comorbidity with AF in ischemic heart failure (Li 2021).

AF is a disease with many origin points. Not all known genetic associations should be expected to be present in a transgenic goat model of cardiac fibrosis. Though perplexing that not all TGF-β1 pathway-related genes investigated were upregulated, there are many nuances in the regulation of the pathway, namely regulation of fibroblast activation through the SMAD protein family, that could account for the lack of differential expression between treatments (Gu 2013). Another potential factor contributing to the lack of significance in some genes could be because both goat groups ranged in age from three to six years; as fully mature and older animals, fibrosis could be increased simply due to age (Biernacka 2011). We investigated this with an unpublished study assessing fibrosis levels in aged WT and TG goats, finding no correlation with fibrosis in aging goat hearts in either unmodified or modified hearts.

This study shows that a large animal model of cardiac fibrosis can help elucidate the effects of fibrosis on AF. These data support our previous findings that fibrosis expressed in the atria of TG goats is likely to come from TGF-β1 overexpression in its active form rather than an inflammation background, and that fibrosis can sustain AF inducibility. The data shown here is difficult to extrapolate to humans as the typical clinical presentation of AF does not come with overexpression of TGF-β1. Performing more in depth electrophysiological studies, such as optical mapping, or patch clamping cardiomyocytes, should be explored to gain more understanding of the cellular behavior within a fibrotic substrate and how cellular communication is impacted. Targeting more clinically relevant genes to generate different large animal models could further contribute to improve the treatment of this condition in clinical practice. Looking deeper molecularly, such as utilizing single cell RNA sequencing, *in* situ hybridization, or isolating and sorting cardiomyocytes may allow for even more insight into the role of fibrosis in AF, such studies should be performed to fully elucidate this effect. If additional clinically relevant large animal models are developed, a better understanding of the genesis and perpetuation of AF can be understood.

More work should be done to characterize the full effect that TGF-β1 induced fibrosis has on cardiac tissue and how that shapes the conductivity of the heart in clinical practice. More refined gene expression could be performed based on the data presented here in order to fully elucidate the mechanisms behind the TGF-β1 cascade in these goats and what effect the transgene has on the phenotype of these animals. This study exhibits how cardiac substrate influences conductivity, and therefore, functionality of the heart. Tissue models have shown that uneven deposition of fibrosis can lead to functional barriers of electrical signal, prompting an increase in self-sustaining re-entrant electrical patterns, promoting arrythmogenesis (Colman 2023). Further, external physiologic factors may serve as a “second hit”, or trigger for sustained AF episodes with a fibrotic substrate present as our group showed with endurance exercise in this goat model (Regouski 2019). A fibrotic, or poorly conducting atria may not be enough to produce an arrythmia spontaneously, but coupled with factors such as exercise or aging may present enough overload to promote an arrhythmogenic state. Increased structural anisotropy may shed more light into the substrate plus trigger concept routinely discussed in atrial fibrillation research. The heterogeneity of atrial fibers, differences in fiber direction leading to

disorganized electrical conduction is found in the TG goats used in this study which may explain why some animals are more inducible than others, particularly with sustained AF episodes (Kwan 2024). This insight may exhibit how disorganized atrial tissue leads to a predisposition to AF, while other “triggering” events may promote the arrhythmia, such as exercise. Looking at ion channels via cardiomyocyte patch clamping may be helpful to understand if an over-expression of TGF-β1 alters these specialized cells themselves, or if the AF observed in these animals comes strictly from excessive fibrosis in the atria. Further studies investigating specific effects from environmental triggers may help contribute to the overall understanding of the development of AF and could be extrapolated to humans.

This body of work showcases the development of a transgenic large animal model of cardiac fibrosis, the first of its kind. There is also strong evidence that structural remodeling on its own without insult or injury can initiate and sustain an AF phenotype without constant perturbation by inflammation, proving important to understand some components of the development of the disease.

Declarations

Author Contribution

M.R. contributed to the conceptualization, methodology, analysis, and writing of the manuscriptH.R., I.A.P., M.J.C. contributed to the conceptualization, methodology, analysis and reviewing and editing the manuscriptA.V.W. provided data collection and images for Figure 4A.T., A.V.W., H.R., I.A.P., M.J.C. contributed conceptualization and validation of the experimentsA.S., C.M., J.F., R.L., R.S., T.P. all assisted with data collectionI.A.P. serves as a corresponding authorAll authors reviewed the manuscript.

Data Availability

All data supporting the findings of this study are available within the paper and its Supplementary Information.

References

1. Al-U'datt D, Allen BG, Nattel S. Role of the lysyl oxidase enzyme family in cardiac function and disease. *Cardiovasc Res*. 2019;115:1820–1837. doi: 10.1093/cvr/cvz176Benjamini Y, Hochberg Y. Controlling the False Discovery Rate: A Practical and Powerful Approach to Multiple Testing. *Journal of the Royal Statistical Society: Series B (Methodological)*. 2018;57:289–300. doi: 10.1111/j.2517-6161.1995.tb02031.x
2. Biernacka A, Frangogiannis NG. Aging and Cardiac Fibrosis. *Aging Dis*. 2011;2:158–173.
3. Boeuf S, Bovée JV, Lehner B, van den Akker B, van Ruler M, Cleton-Jansen AM, Richter W. BMP and TGFbeta pathways in human central chondrosarcoma: enhanced endoglin and Smad 1 signaling in high grade tumors. *BMC Cancer*. 2012;12:488. doi: 10.1186/1471-2407-12-488

4. Bolivar S, Espitia-Corredor JA, Olivares-Silva F, Valenzuela P, Humeres C, Anfossi R, Castro E, Vivar R, Salas-Hernández A, Pardo-Jiménez V, et al. In cardiac fibroblasts, interferon-beta attenuates differentiation, collagen synthesis, and TGF-β1-induced collagen gel contraction. *Cytokine*. 2021;138:155359. doi: 10.1016/j.cyto.2020.155359
5. Brundel B, Ai X, Hills MT, Kuipers MF, Lip GYH, de Groot NMS. Atrial fibrillation. *Nat Rev Dis Primers*. 2022;8:21. doi: 10.1038/s41572-022-00347-9
6. Büttner P, Ueberham L, Shoemaker MB, Roden DM, Dinov B, Hindricks G, Bollmann A, Husser D. Identification of Central Regulators of Calcium Signaling and ECM-Receptor Interaction Genetically Associated With the Progression and Recurrence of Atrial Fibrillation. *Front Genet*. 2018;9:162. doi: 10.3389/fgene.2018.00162
7. Castro F, Cardoso AP, Gonçalves RM, Serre K, Oliveira MJ. Interferon-Gamma at the Crossroads of Tumor Immune Surveillance or Evasion. *Front Immunol*. 2018;9:847. doi: 10.3389/fimmu.2018.00847
8. Chen X, Xu J, Jiang B, Liu D. Bone Morphogenetic Protein-7 Antagonizes Myocardial Fibrosis Induced by Atrial Fibrillation by Restraining Transforming Growth Factor-β (TGF-β)/Smads Signaling. *Med Sci Monit*. 2016;22:3457–3468. doi: 10.12659/msm.897560
9. Cheng T, Wang XF, Hou YT, Zhang L. Correlation between atrial fibrillation, serum amyloid protein A and other inflammatory cytokines. *Mol Med Rep*. 2012;6:581–584. doi: 10.3892/mmr.2012.934
10. Colman, MA, Sharma R, Aslandi OV, Zhao J. Patchy fibrosis promotes trigger-substrate interactions that both generate and maintain atrial fibrillation. *Interface Focus.* 2023; 13. doi: 10.1098/rsfs.2023.0041
11. de Oliveira Camargo R, Abual'anaz B, Rattan SG, Filomeno KL, Dixon IMC. Novel factors that activate and deactivate cardiac fibroblasts: A new perspective for treatment of cardiac fibrosis. *Wound Repair Regen*. 2021;29:667–677. doi: 10.1111/wrr.12947
12. de Pater E, Ciampricotti M, Priller F, Veerkamp J, Strate I, Smith K, Lagendijk AK, Schilling TF, Herzog W, Abdelilah-Seyfried S, et al. Bmp signaling exerts opposite effects on cardiac differentiation. *Circ Res*. 2012;110:578–587. doi: 10.1161/circresaha.111.261172
13. Farhan A, Latif MA, Minhas A, Weiss CR. Cardiac and Hemodynamic Manifestations of Hereditary Hemorrhagic Telangiectasia. *Int J Angiol*. 2022;31:75–82. doi: 10.1055/s-0042-1745842
14. Frangogiannis NG. Cardiac fibrosis: Cell biological mechanisms, molecular pathways and therapeutic opportunities. *Mol Aspects Med*. 2019;65:70–99. doi: 10.1016/j.mam.2018.07.001
15. Frangogiannis N. Transforming growth factor-β in tissue fibrosis. *J Exp Med*. 2020;217:e20190103. doi: 10.1084/jem.20190103
16. Glasscock E, Voigt N, McCauley MD, Sun Q, Li N, Chiang DY, Zhou XB, Molina CE, Thomas D, Schmidt C, et al. Expression and function of Kv1.1 potassium channels in human atria from patients with atrial fibrillation. *Basic Res Cardiol*. 2015;110:505. doi: 10.1007/s00395-015-0505-6
17. Gramley F, Lorenzen J, Jedamzik B, Gatter K, Koellensperger E, Munzel T, Pezzella F. Atrial fibrillation is associated with cardiac hypoxia. *Cardiovasc Pathol*. 2010;19:102–111. doi:

10.1016/j.carpath.2008.11.001

18. Gu J, Liu X, Wang QX, Guo M, Liu F, Song ZP, Zhang DD. Beneficial effects of pioglitazone on atrial structural and electrical remodeling in vitro cellular models. *J Mol Cell Cardiol*. 2013;65:1–8. doi: 10.1016/j.yjmcc.2013.09.016
19. Guan YZ, Liu H, Huang HJ, Liang DY, Wu SY, Zhang T. Identification of the Potential Molecular Mechanism of TGFBI Gene in Persistent Atrial Fibrillation. *Comput Math Methods Med*. 2022;2022:1643674. doi: 10.1155/2022/1643674
20. Guo YH, Yang YQ. Atrial Fibrillation: Focus on Myocardial Connexins and Gap Junctions. *Biology (Basel)*. 2022;11. doi: 10.3390/biology11040489
21. Heijman J, Muna AP, Veleva T, Molina CE, Sutanto H, Tekook M, Wang Q, Abu-Taha IH, Gorka M, Künzel S, et al. Atrial Myocyte NLRP3/CaMKII Nexus Forms a Substrate for Postoperative Atrial Fibrillation. *Circ Res*. 2020;127:1036–1055. doi: 10.1161/circresaha.120.316710
22. Hoffmann S, Paone C, Sumer SA, Diebold S, Weiss B, Roeth R, Clauss S, Klier I, Kääb S, Schulz A, et al. Functional Characterization of Rare Variants in the SHOX2 Gene Identified in Sinus Node Dysfunction and Atrial Fibrillation. *Front Genet*. 2019;10:648. doi: 10.3389/fgene.2019.00648
23. Hogan BL. Bone morphogenetic proteins: multifunctional regulators of vertebrate development. *Genes Dev*. 1996;10:1580–1594. doi: 10.1101/gad.10.13.1580
24. Hu W, Xin Y, Zhao Y, Hu J. Shox2: The Role in Differentiation and Development of Cardiac Conduction System. *Tohoku J Exp Med*. 2018;244:177–186. doi: 10.1620/tjem.244.177
25. Hu YF, Chen YJ, Lin YJ, Chen SA. Inflammation and the pathogenesis of atrial fibrillation. *Nat Rev Cardiol*. 2015;12:230–243. doi: 10.1038/nrcardio.2015.2
26. Humeres C, Shinde AV, Hanna A, Alex L, Hernández SC, Li R, Chen B, Conway SJ, Frangogiannis NG. Smad7 effects on TGF-β and ErbB2 restrain myofibroblast activation and protect from postinfarction heart failure. *J Clin Invest*. 2022;132. doi: 10.1172/jci146926Kay JM. Comparative morphologic features of the pulmonary vasculature in mammals. *Am Rev Respir Dis*. 1983;128:S53-57. doi: 10.1164/arrd.1983.128.2P2.S53
27. Koroghli JA, Floyd E, Regouski M, Rood K, Gash K, Panter K, Stott R, Davies CJ, Polejaeva IA, Rutigliano HM. Gene expression and lymphocyte population at the fetal-maternal interface in sheep pregnancies established by somatic cell nuclear transfer. *Reprod Fertil Dev*. 2018;30:1011–1020. doi: 10.1071/RD17224
28. Kwan E, Ghafoori E, Good W, Regouski M, Moon B, Fish JM, Hsu E, Polejaeva IA, MacLeod RS, Dosdall DJ, Ranjan R. Diffuse functional and structural abnormalities in fibrosis: Potential structural basis for sustaining atrial fibrillation. *Heart Rhythm*. 2024;18:1547–5271. doi: 10.016/j.hrthm.2024.10.060
29. Kwan E, Hunt B, Paccione E, Orkild BA, Bergquist JA, Yazaki K, Polejaeva I, Hsu E, Dosdall D, MacLeod RS, Ranjan R. Structural Differences in Transgenic Animals Associated with Atrial Fibrillation. Comput Cardiol (2010). 2024 Sep;51:10.22489/cinc.2024.414. doi: 10.22489/cinc.2024.414.

30. Lambiase PD, Tinker A. Connexins in the heart. *Cell Tissue Res*. 2015;360:675–684. doi: 10.1007/s00441-014-2020-8
31. Li H, Sun W, Wang Z, Wang Z, Du X, Chen J, Gao J, Liu X, Wang X, Wang Y, et al. Higher serum tissue inhibitor of metalloproteinase-1 predicts atrial fibrillation recurrence after radiofrequency catheter ablation. *Front Cardiovasc Med*. 2022;9:961914. doi: 10.3389/fcvm.2022.961914
32. Li Z, Zhao H, Wang J. Metabolism and Chronic Inflammation: The Links Between Chronic Heart Failure and Comorbidities. *Front Cardiovasc Med*. 2021;8:650278. doi: 10.3389/fcvm.2021.650278
33. Oikonomou E, Zografos T, Papamikroulis GA, Siasos G, Vogiatzi G, Theofilis P, Briasoulis A, Papaioannou S, Vavuranakis M, Gennimata V, et al. Biomarkers in Atrial Fibrillation and Heart Failure. *Curr Med Chem*. 2019;26:873–887. doi: 10.2174/0929867324666170830100424
34. Olsen FJ, Bertelsen L, Knegt MCd, Christensen TE, Vejlstrup N, Svendsen JH, Jensen JS, Biering-Sørensen T. Multimodality Cardiac Imaging for the Assessment of Left Atrial Function and the Association With Atrial Arrhythmias. *Circulation: Cardiovascular Imaging*. 2016;9:e004947. doi: doi:10.1161/CIRCIMAGING.116.004947
35. Park E, Cho M, Ki CS. Correct use of repeated measures analysis of variance. *Korean J Lab Med*. 2009;29:1–9. doi: 10.3343/kjlm.2009.29.1.1
36. Petersen AM, Pedersen BK. The anti-inflammatory effect of exercise. *J Appl Physiol (1985)*. 2005;98:1154–1162. doi: 10.1152/japplphysiol.00164.2004
37. Polejaeva IA, Ranjan R, Davies CJ, Regouski M, Hall J, Olsen AL, Meng Q, Rutigliano HM, Dosdall DJ, Angel NA, et al. Increased Susceptibility to Atrial Fibrillation Secondary to Atrial Fibrosis in Transgenic Goats Expressing Transforming Growth Factor-beta1. *J Cardiovasc Electrophysiol*. 2016;27:1220–1229. doi: 10.1111/jce.13049
38. Regouski M, Galenko O, Doleac J, Olsen AL, Jacobs V, Liechty D, White KL, Bunch TJ, Lee PM, Rutigliano HM, et al. Spontaneous Atrial Fibrillation in Transgenic Goats With TGF (Transforming Growth Factor)-beta1 Induced Atrial Myopathy With Endurance Exercise. *Circ Arrhythm Electrophysiol*. 2019;12:e007499. doi: 10.1161/CIRCEP.119.007499
39. Robertson IB, Horiguchi M, Zilberberg L, Dabovic B, Hadjiolova K, Rifkin DB. Latent TGF-β-binding proteins. *Matrix Biol*. 2015;47:44–53. doi: 10.1016/j.matbio.2015.05.005
40. Rose BA, Force T, Wang Y. Mitogen-activated protein kinase signaling in the heart: angels versus demons in a heart-breaking tale. *Physiol Rev*. 2010;90:1507–1546. doi: 10.1152/physrev.00054.2009
41. Roselli C, Chaffin MD, Weng LC, Aeschbacher S, Ahlberg G, Albert CM, Almgren P, Alonso A, Anderson CD, Aragam KG, et al. Multi-ethnic genome-wide association study for atrial fibrillation. *Nat Genet*. 2018;50:1225–1233. doi: 10.1038/s41588-018-0133-9
42. Schroder K, Hertzog PJ, Ravasi T, Hume DA. Interferon-gamma: an overview of signals, mechanisms and functions. *J Leukoc Biol*. 2004;75:163–189. doi: 10.1189/jlb.0603252
43. Shan X, Liu Z, Wulasihan M, Ma S. Edoxaban improves atrial fibrillation and thromboembolism through regulation of the Wnt-β-induced PI3K/ATK-activated protein C system. *Exp Ther Med*. 2019;17:3509–3517. doi: 10.3892/etm.2019.7379

44. Sumer SA, Hoffmann S, Laue S, Campbell B, Raedecke K, Frajs V, Clauss S, Kääb S, Janssen JWG, Jauch A, et al. Precise Correction of Heterozygous SHOX2 Mutations in hiPSCs Derived from Patients with Atrial Fibrillation via Genome Editing and Sib Selection. *Stem Cell Reports*. 2020;15:999–1013. doi: 10.1016/j.stemcr.2020.08.015
45. Tsai CT, Hsieh CS, Chang SN, Chuang EY, Ueng KC, Tsai CF, Lin TH, Wu CK, Lee JK, Lin LY, et al. Genome-wide screening identifies a KCNIP1 copy number variant as a genetic predictor for atrial fibrillation. *Nat Commun*. 2016;7:10190. doi: 10.1038/ncomms10190
46. van den Berg NWE, Neefs J, Kawasaki M, Nariswari FA, Wesselink R, Fabrizi B, Jongejan A, Klaver MN, Havenaar H, Hulsman EL, et al. Extracellular matrix remodeling precedes atrial fibrillation: Results of the PREDICT-AF trial. *Heart Rhythm*. 2021;18:2115–2125. doi: 10.1016/j.hrthm.2021.07.059
47. Wynn TA, Ramalingam TR. Mechanisms of fibrosis: therapeutic translation for fibrotic disease. *Nat Med*. 2012;18:1028–1040. doi: 10.1038/nm.2807
48. Yang M, Hall J, Fan Z, Regouski M, Meng Q, Rutigliano HM, Stott R, Rood KA, Panter KE, Polejaeva IA. Oocytes from small and large follicles exhibit similar development competence following goat cloning despite their differences in meiotic and cytoplasmic maturation. *Theriogenology*. 2016;86:2302–2311. doi: 10.1016/j.theriogenology.2016.07.026
49. Yang M, Perisse I, Fan Z, Regouski M, Meyer-Ficca M, Polejaeva IA. Increased pregnancy losses following serial somatic cell nuclear transfer in goats. *Reprod Fertil Dev*. 2018. doi: 10.1071/RD17323
50. Ye D, Liu Y, Pan H, Feng Y, Lu X, Gan L, Wan J, Ye J. Insights into bone morphogenetic proteins in cardiovascular diseases. *Frontiers in Pharmacology*. 2023;14. doi: 10.3389/fphar.2023.1125642
51. Zhou J, Dong Y, Cai X, Yang H, Guo T. Identification and Validation of Autophagy-Related Genes as Potential Biomarkers and Therapeutic Targets in Atrial Fibrillation. *Int J Gen Med*. 2021;14:7783–7796. doi: 10.2147/ijgm.S337855
52. Zhu Y, Chen L, Song B, Cui Z, Chen G, Yu Z, Song B. Insulin-like Growth Factor-2 (IGF-2) in Fibrosis. *Biomolecules*. 2022;12. doi: 10.3390/biom12111557

Figures

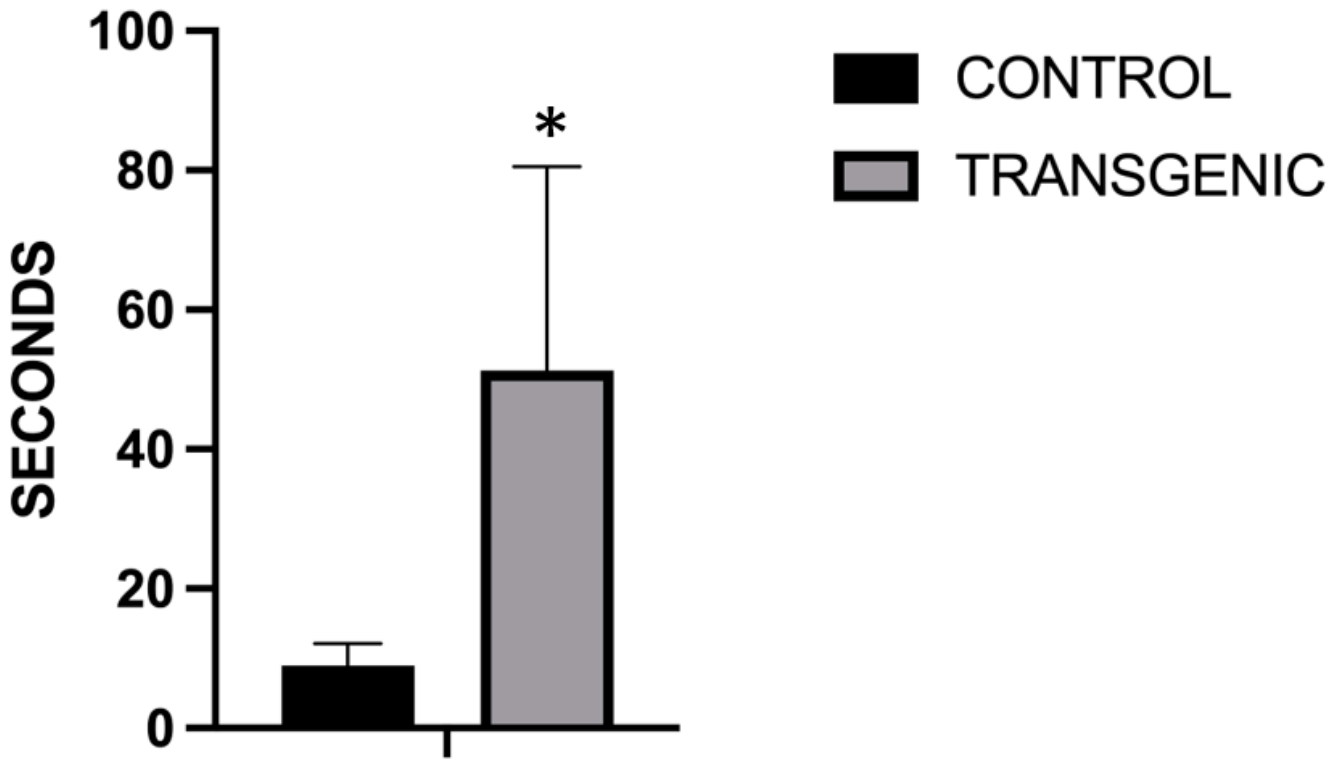


Figure 1

Average atrial fibrillation (AF) duration of TGF-b1 transgenic animals (TG, n=6) when compared to their wild-type (WT, n=6) controls. Average duration in seconds at baseline is significantly upregulated in TG animals when compared to their WT controls, as denoted by the symbol *. WT animals had an average induced AF duration of 8.98 ± 3.18 seconds, whereas TG animals had an average of 51.30 ± 29.27 seconds (*p*=0.04*)* when analyzed using a Student's t-test.Data are expressed as mean ± SEM.

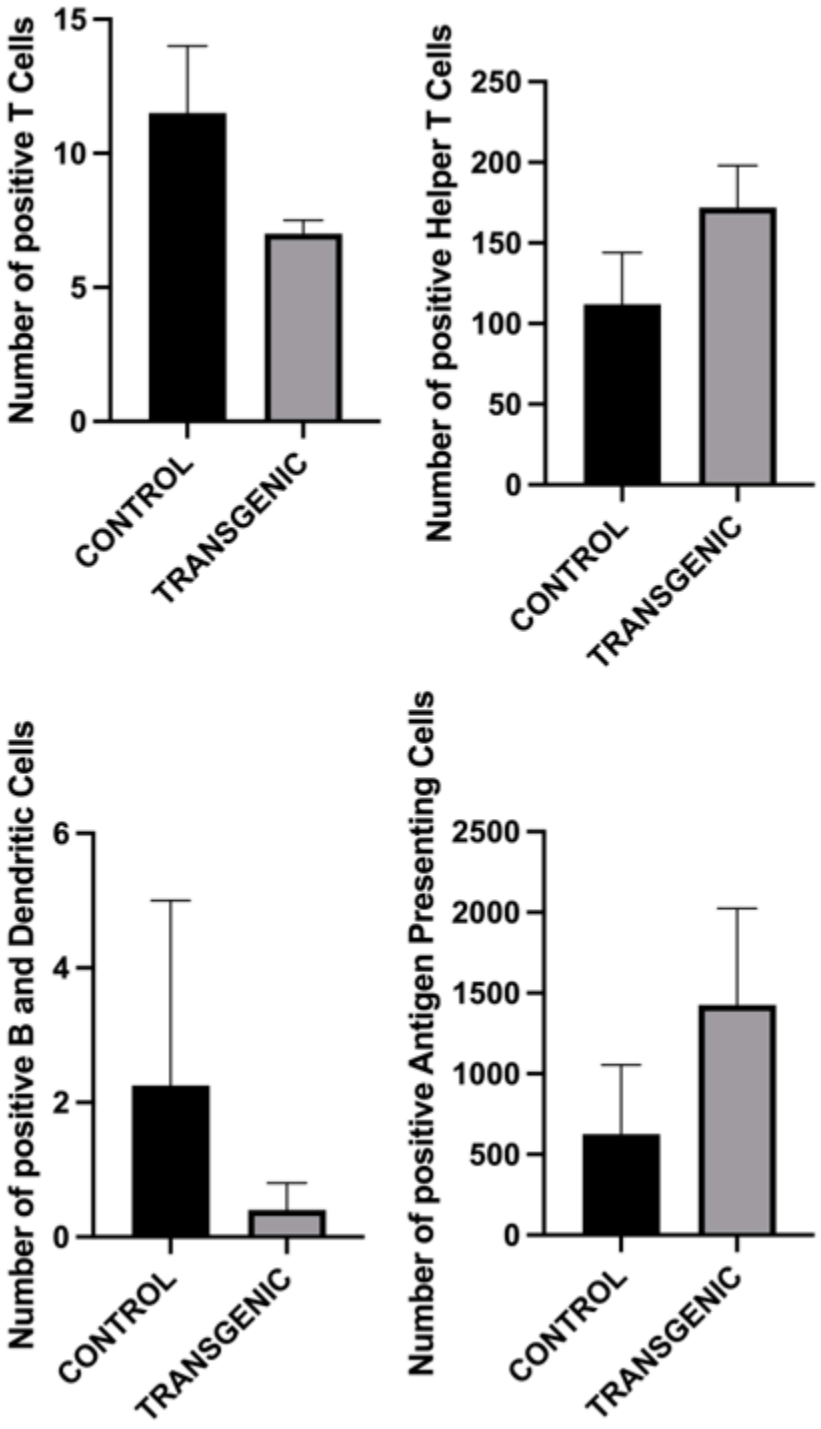


Figure 2

Analysis of immune cell populations in the right atrium of human TGF-b1 transgenic (TG, n=6) goats compared to age and sex matched wild-type (WT, n=6) control goats via immunohistochemistry staining. No significant differences were found between groups using a Student's t-test. The number of T cells (CD2+) had a significance level of *p=0.19*, the number of T helper cells (CD4+) had a significance level of *p=0.13*, the number of B cells (CD21+) had a significance level of *p=0.36*, and finally, the number of

antigen-presenting cells (MHC-II+) had a significance level of *p=0.39.* Data are presented as average ±SEM.

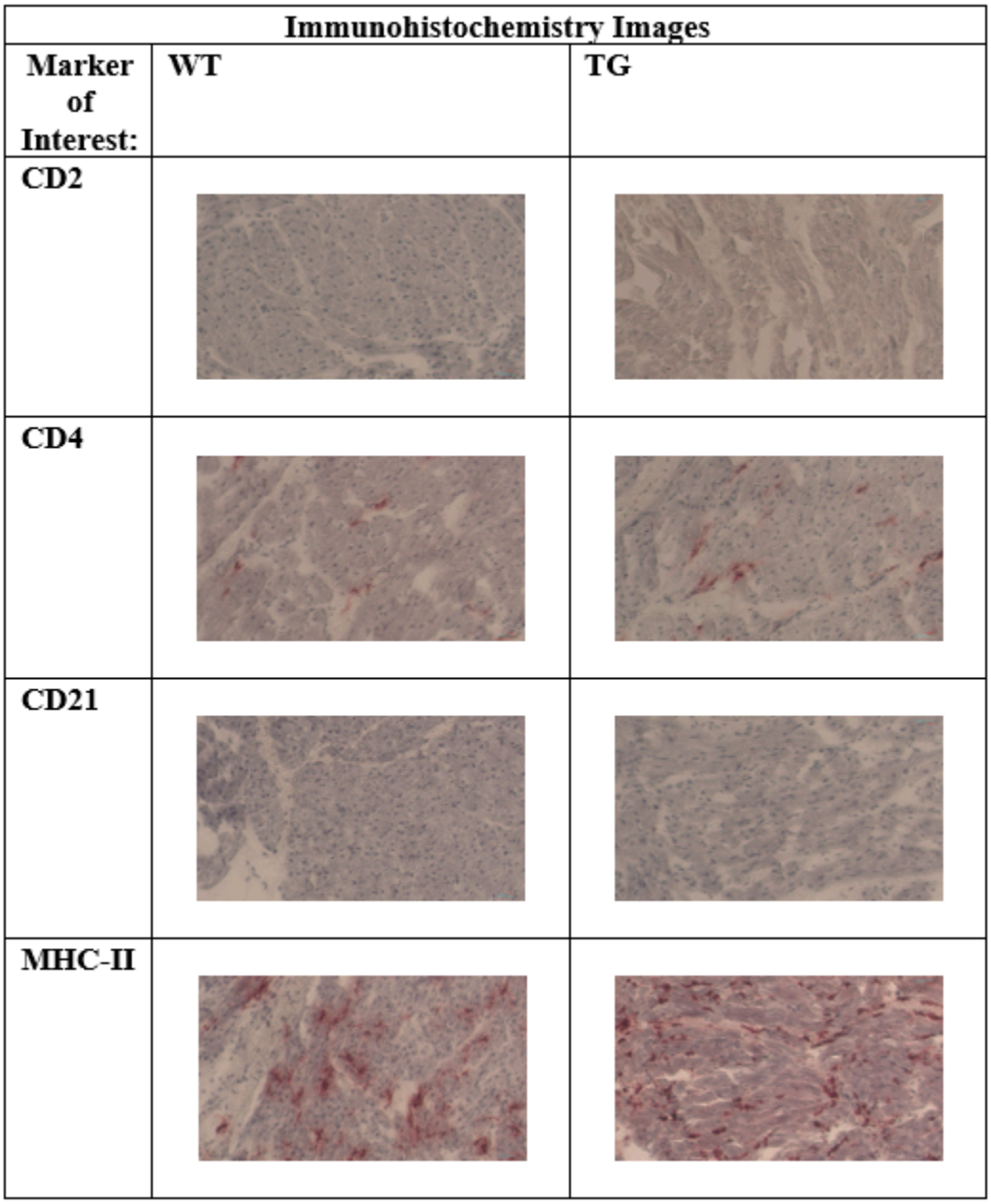


Figure 3

Immunohistochemical labeling of cells for CD2, CD4, CD21, and MHC-II in the atrium of TGF-b1transgenic (TG) and age and sex matched wild-type (WT) control goat atrial samples. Using a Zeiss Axio Observer Z1 (Zeiss, Hebron, KY, USA) microscope, ten fields of view at 400x objective were visualized for the presence of positive cells from antibody staining and the number of positive cells per area was recorded.

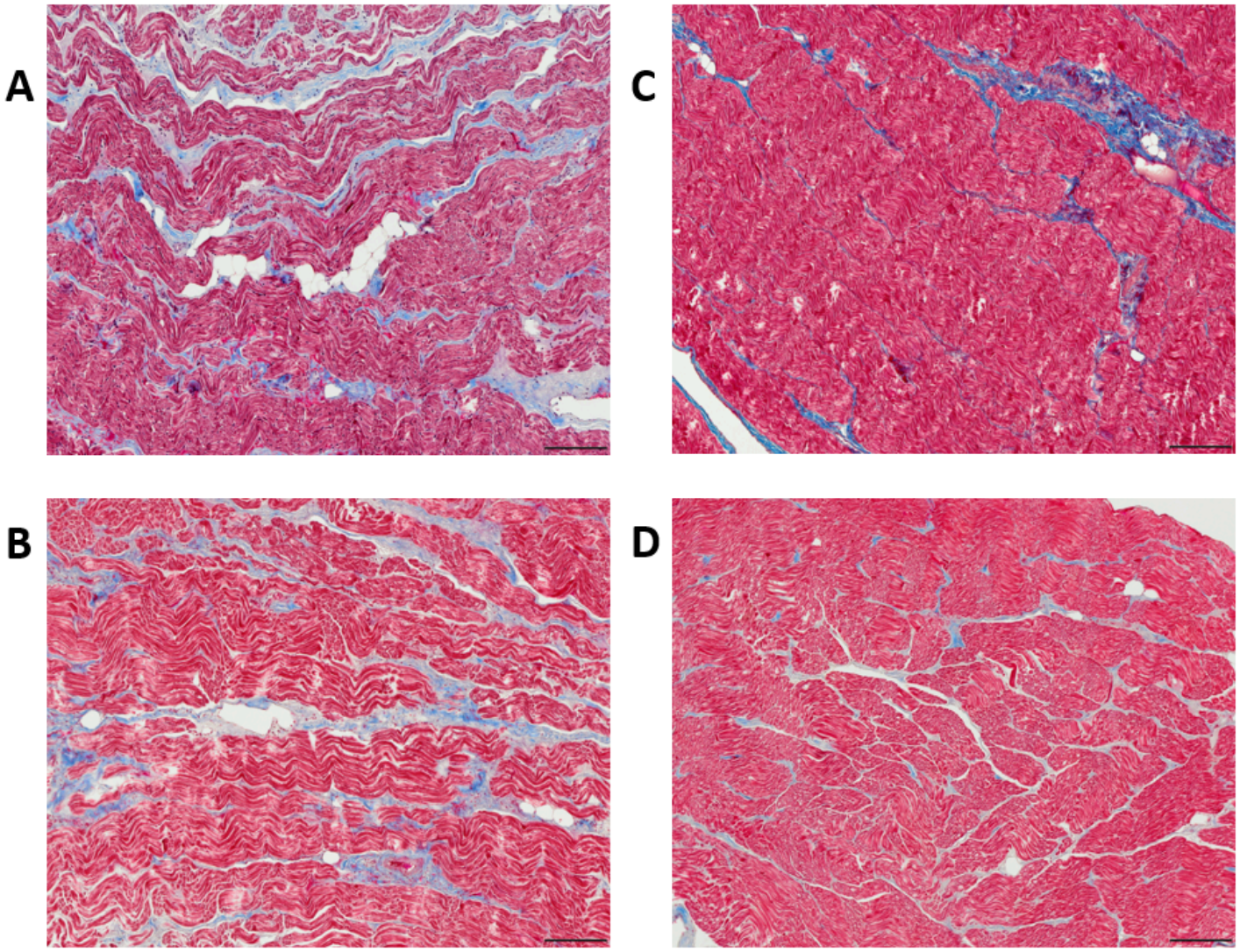


Figure 4

Representative images of Masson's Trichrome staining of atrial tissue from two TGF-b1transgenic goats in panel A and B and two age and sex matched wild-type control goat atrial tissue in panel C and D. 40x scale bar=500mm. Images were analyzed using Photoshop to obtain the percent fibrosis. Using the Mann-Whitney U test, percent fibrosis was significantly higher in TG hearts (TG, n=8) compared to WT controls (WT, n=7): median [IQR]: TG 6.5% (4-9%), WT 2% (0-2%), U=56, p=0.0014.

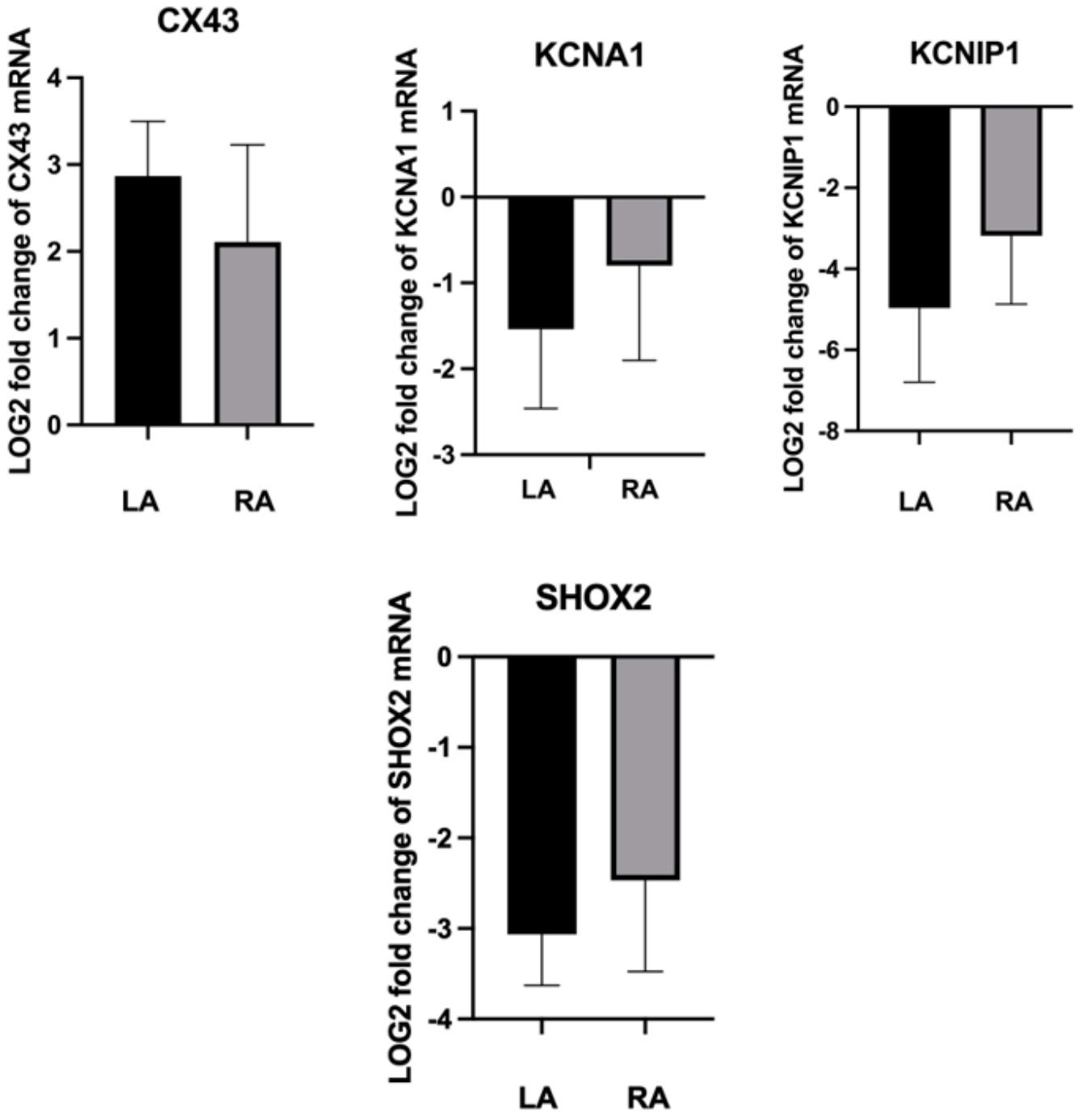


Figure 5

Fold change of gene expression of atrial fibrillation (AF) related genes showing significant difference between TGF-b1transgenic (TG; n=6) and age and sex matched wild-type (WT; n=6) control goat atrial samples. Graphs represent 2^-DDCT fold change in relative mRNA transcript levels in TG animals detected using qRT-PCR, values were normalized to mRNA transcript levels of glyceraldehyde-3-phosphate dehydrogenase (GAPDH) and actin beta (ACTB) and to WT animal transcript level for the individual target gene. After a false discovery rate adjustment of significant values, and a fold change cut

off of 1.5 applied: CX43 has a significance level of *p=0.003 KCNA1 p=0.012, KCNIP1 p=0.009, SHOX2 p=0.02.* Non-adjusted *p* values can be found in Table 2. Data are expressed as mean ± SEM.

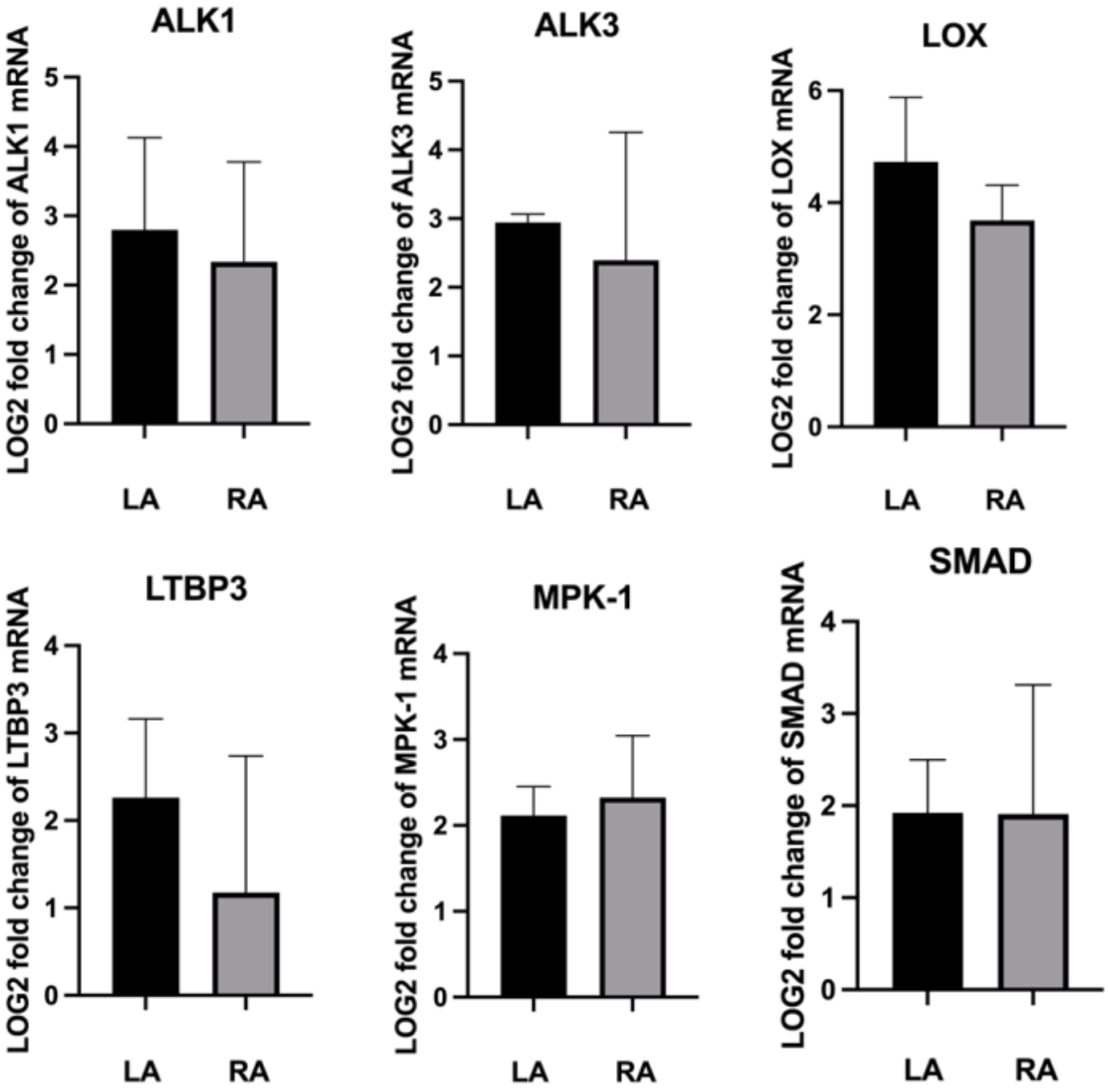


Figure 6

Fold change of gene expression of TGFb-1 related genes showing significant difference between TGF-b1transgenic (TG; n=6) and age and sex matched wild-type (WT; n=6) control goat atrial samples. Graphs represent 2^-DDCT fold change in relative mRNA transcript levels in TG animals detected using qRT-PCR, values were normalized to mRNA transcript levels of glyceraldehyde-3-phosphate dehydrogenase (GAPDH) and actin beta (ACTB) and to WT animals transcript level for the individual target gene. After a

false discovery rate adjustment of significant values and a fold change cut off of 1.5 applied, *ALK1* has a significance of *p=0.003, ALK3 p=0.002, hTGFb p=0.004, LOX p=0.002, LTBP3 p=0.002, MKP-1 p=0.001, and SMAD* also had a significance level *of p=0.001.* Non-adjusted *p* values can be found in Table 2. Data are expressed as mean ± SEM.

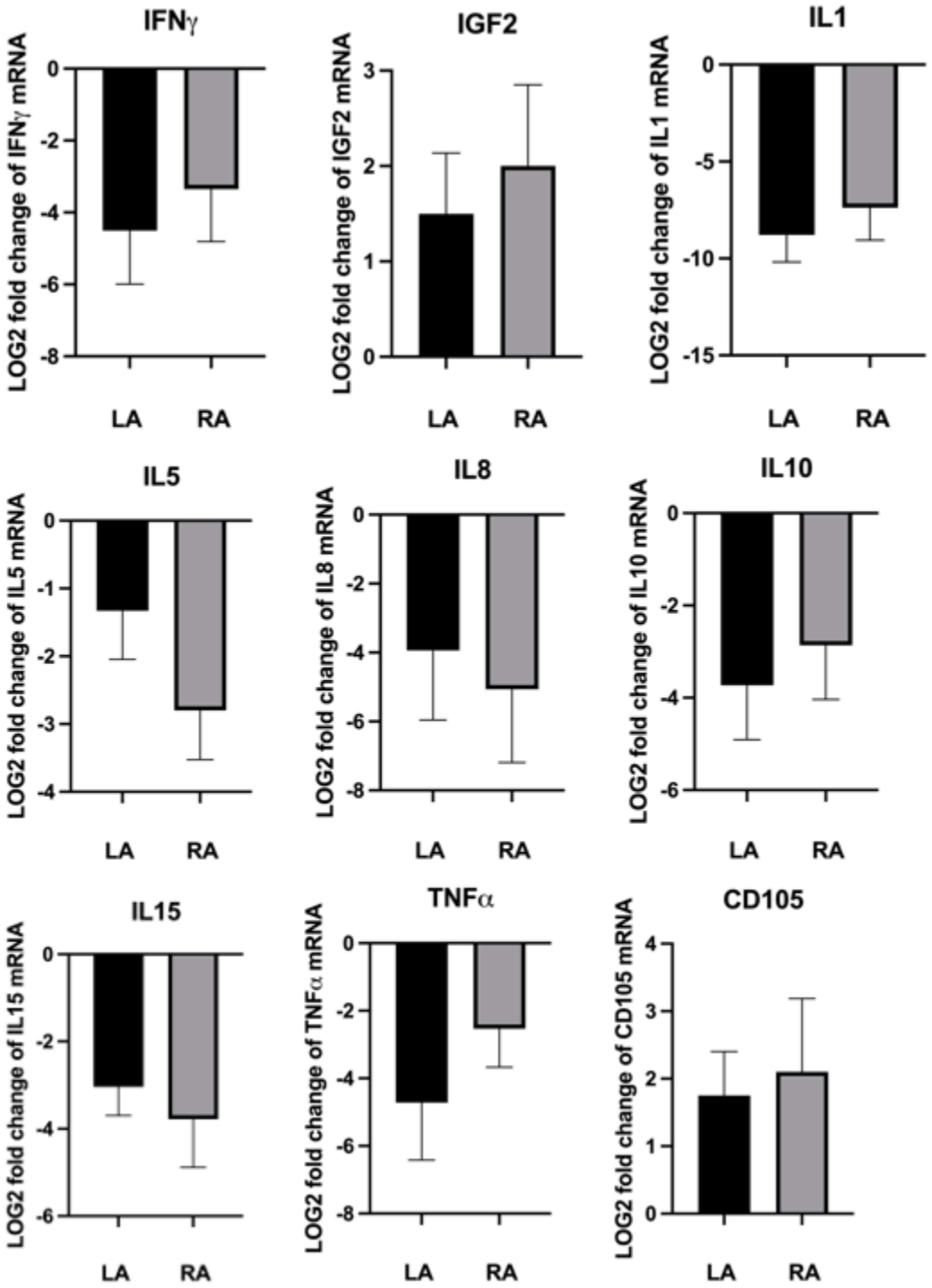


Figure 7

Fold change of gene expression of inflammation-related genes showing significant difference between TGF-b1 transgenic (TG; n=6) and age and sex matched wild-type (WT; n=6) control goat atrial samples. Graphs represent 2^-DDCT fold change in relative mRNA transcript levels in TG animals detected using qRT-PCR, values were normalized to mRNA transcript levels of glyceraldehyde-3-phosphate dehydrogenase (GAPDH) and actin beta (ACTB) and to WT animal transcript level for the individual target gene. After a false discovery rate adjustment of significant values and a fold change cut off of 1.5 applied, *CD105* had of*p=0.002, IFNg p=0.005, IGF2 p=0.002, IL1 p=0.001, IL5 p=0.002, , IL8 p=0.001, IL10 p=0.004, IL15 P=0.003 and TNFa* also had a significance level *of p=0.001.* Non-adjusted *p* values can be found in Table 2. Data are expressed as mean ± SEM.

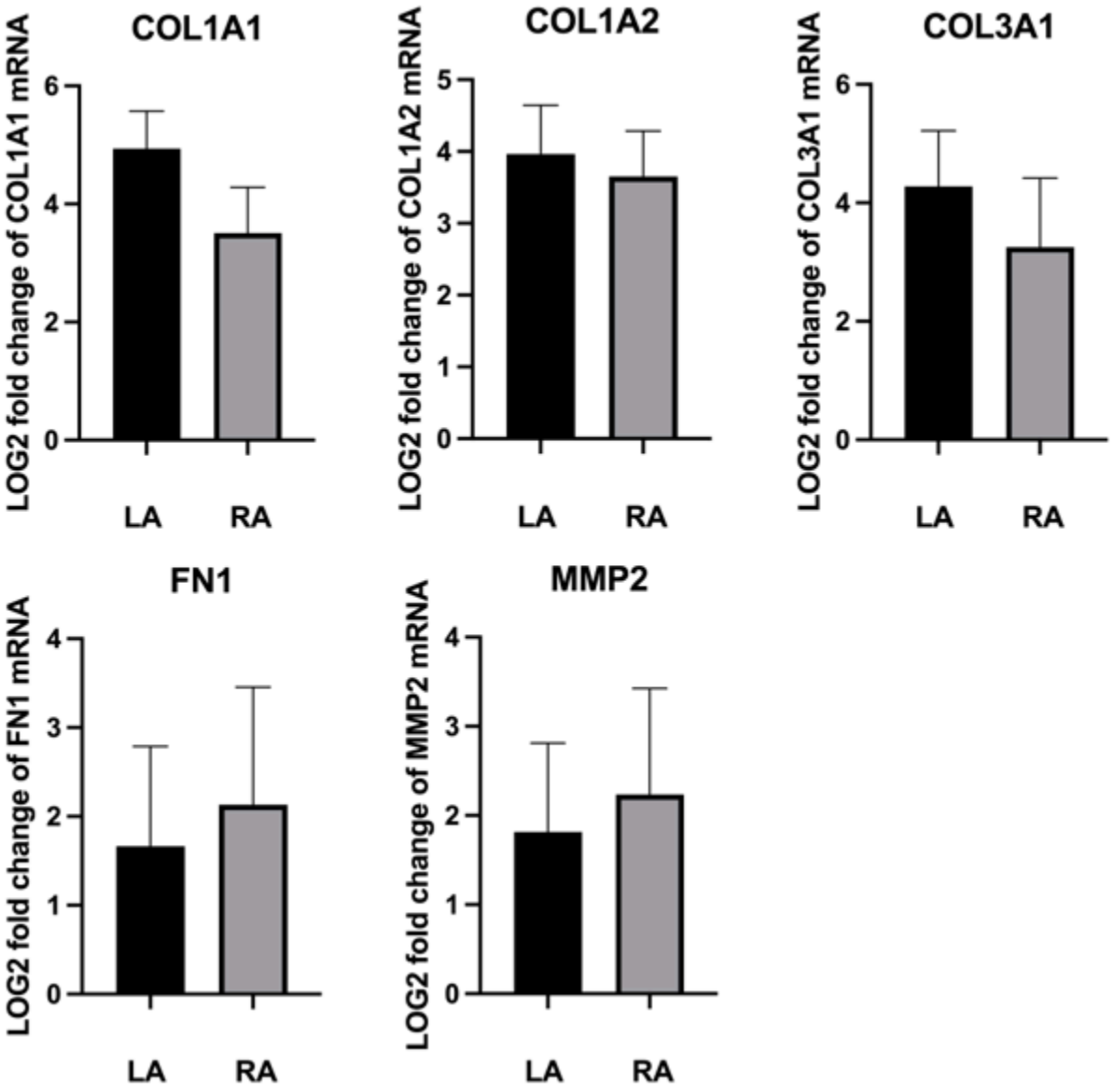


Figure 8

Fold change of gene expression of extra cellular matrix related genes showing significant difference between TGF-b1transgenic (TG; n=6) and age and sex matched wild-type (WT; n=6) control goat atrial samples. Graphs represent 2^-DDCT fold change in relative mRNA transcript levels in TG animals detected using qRT-PCR, values were normalized to mRNA transcript levels of glyceraldehyde-3-phosphate dehydrogenase (GAPDH) and actin beta (ACTB) and to WT animal transcript level for the individual target gene. After a false discovery rate adjustment of significant values and a fold change cut off of 1.5 applied, *COL1A1* has a significance of *p=0.003, COL1A2 p=0.002, COL3A1 p=0.002, FN1 p=0.005, and MMP2* also had a significance level *of p=0.001.* Non-adjusted *p*values can be found in Table 2. Data are expressed as mean ± SEM.